Langmuir

Article

pubs.acs.org/Langmuir

Antibacterial Activity and Biosensing of PVA-Lysozyme Microbubbles Formed by Pressurized Gyration

Suntharavathanan Mahalingam, Zewen Xu, and Mohan Edirisinghe*

Department of Mechanical Engineering, University College London, Torrington Place, London WC1E 7JE, U.K.

Supporting Information

ABSTRACT: In this work, the biosensing and antibacterial capabilities of PVA-lysozyme microbubbles have been explored. Gas-filled PVA-lysozyme microbubbles with and without gold nanoparticles in the diameter range of 10 to 250 μm were produced using a single-step pressurized gyration process. Fluorescence microscopy showed the integration of gold nanoparticles on the shell of the microbubbles. Microbubbles prepared with gold nanoparticles showed greater optical extinction values than those without gold nanoparticles, and these values increased with the concentration of the gold nanoparticles. Both types of microbubbles showed antibacterial activity against Gram-negative *Escherichia coli* (*E. coli*), with the bubbles containing the gold nanoparticles performing better than the former. The conjugation of the microbubbles with alkaline phosphatase allowed the detection of pesticide paraoxon in aqueous solution, and this demonstrates the biosensing capabilities of these microbubbles.

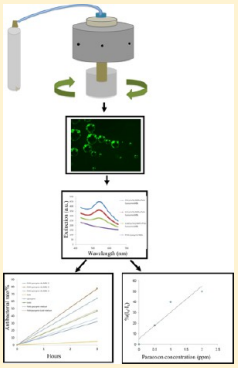

1. INTRODUCTION

Although microbubbles have been extensively explored for clinical imaging and drug delivery purposes,[1−6] little work is reported on their antibacterial and biosensing properties. Microbubbles could either be used to deliver antibiotics to targeted bacterial strains[7] or the microbubbles themselves could be resistant to most of the common bacterial strains found in clinical use.[8] He et al.[9] showed that ultrasound-targeted microbubble destruction could enhance the vancomycin activity against *Staphylococcus epidermidis* biofilms. A microbubble emulsion combined with sonic or ultrasonic agitation showed increased resistance to *Enterococcus faecalis* biofilms and enhanced the antibiofilm efficacy.[10] Sonochemically formed, antibiotics-loaded bovine serum albumin microspheres have been used as antimicrobial agents against *Staphylococcus aureus* (*S. aureus*) and *E. coli* in cotton fabrics.[11] Sun et al.[12] have shown that monodisperse colloidal crystal beads are suitable for multiplex bioassay and could be used in biosensing applications.

Lysozyme, which is an enzyme found in various biological fluids and tissues, has been used to form stable microbubbles for protein and nucleic acid delivery.[13] Lysozyme microbubbles can also partially retain their antimicrobial activity despite their denaturation.[8] The stability of lysozyme microbubbles depends on the denaturation and formation of thiol functional groups and cross-linking.[8,13] Indeed, the stability of microbubbles is determined by the thickness and elasticity of shell material.[14] Microbubble stability could also be achieved by particle "jamming" at the interface[14,15] or interfacial patterning which arrests the shrinkage of bubbles.[16] Alternatively, the stability could be improved by the manipulation of shell composition. The addition of polymers to the formulation will increase the resistance to dissolution.[17] Variation in polymer composition alters the shell properties, thus affecting microbubble shrinkage and destruction.[18]

Pressurized gyration is an emerging technique that utilizes centrifugal force and dynamic fluid flow to jet out microbubbles consistently.[19] In a typical pressurized gyration process, the rotational speed and working pressure of the solution being spun determine the morphology of the product; therefore, careful selection of the operating conditions is vital to the success of the process.[19,20] A map of rotational speed and working pressure has identified the microbubble formation region for PVA-lysozyme protein solutions.[19] It has been shown that below a critical minimum pressure and a critical minimum rotational speed no microbubbles are formed due to either insufficient fluid flow or centrifugal speed. This work also uncovered that the stable optically tunable microbubbles can be prepared by pressurized gyration. Here we explore the biosensing and the antibacterial activity of the PVA-lysozyme microbubbles formed by pressurized gyration.

2. EXPERIMENTAL DETAILS

2.1. Materials. Poly(vinyl alcohol) (PVA) (M_w = 146−186 kDa, 87−89% hydrolyzed) and lysozyme from chicken egg white (M_w = 14.3 kDa, ∼70 000 U/mg) were obtained from Sigma-Aldrich, U.K. Both were used as received without any modification. Gold nanoparticles (average diameter ∼10 nm) in phosphate-buffered saline (PBS) solution were obtained from Sigma-Aldrich, U.K. Alkaline phosphatase, *p*-nitrophenyl phosphate (p-NPP), and paraoxon were purchased from Sigma-Aldrich, U.K.

2.2. Solution Preparation and Characterization. PVA powder was dissolved in distilled water and mixed using a magnetic stirrer for 2

Received: June 2, 2015
Revised: August 17, 2015
Published: August 25, 2015

DOI: 10.1021/acs.langmuir.5b02005
Langmuir 2015, 31, 9771−9780

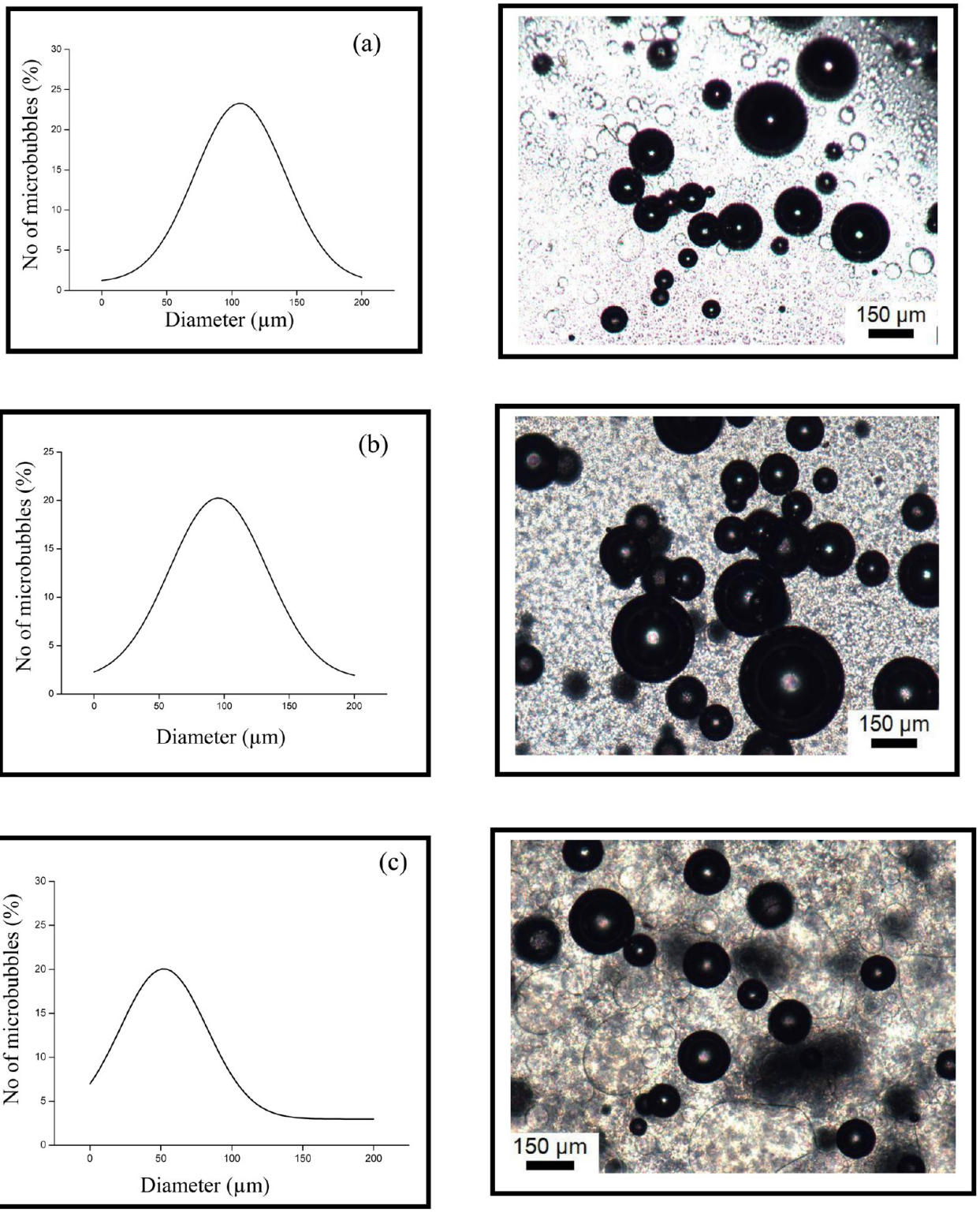

Figure 1. PVA-lysozyme microbubble size distribution and corresponding optical micrograph obtained at rotational speeds (rpm) of (a) 10 000, (b) 24 000, and (c) 36 000. In all instances the working pressure was 0.2×10^5 Pa.

h at 90 °C to prepare the 10% w/v PVA solution. Once the 10% w/v PVA solution was cooled to ∼4 °C, lysozyme powder was dissolved in the PVA solution to produce a 4% w/v solution. Lysozyme was completely dissolved by gentle mixing with a magnetic stirrer to make a homogeneous solution (8 wt % PVA and 4 wt % lysozyme). Although this solution was very viscous (∼720 mPa s) it remained a liquid at ∼4 °C. Once samples were prepared they were stored at 4 °C and were used within 24 h. The gold nanoparticle solution and PVA-lysozyme solution with v/v ratios of 1:10, 1:5, and 2:5 were used to prepare the gold-nanoparticle-containing microbubbles. The solutions were mechanically stirred at 80 °C for 1 h prior to pressurized gyration.

The surface tension and the viscosity of the PVA-lysozyme solutions and PVA-lysozyme solutions containing gold nanoparticles were measured. A Kruss K9 tensiometer was used to measure the static surface tension of the solutions (Wilhelmy plate method). The

DOI: 10.1021/acs.langmuir.5b02005
Langmuir 2015, 31, 9771−9780

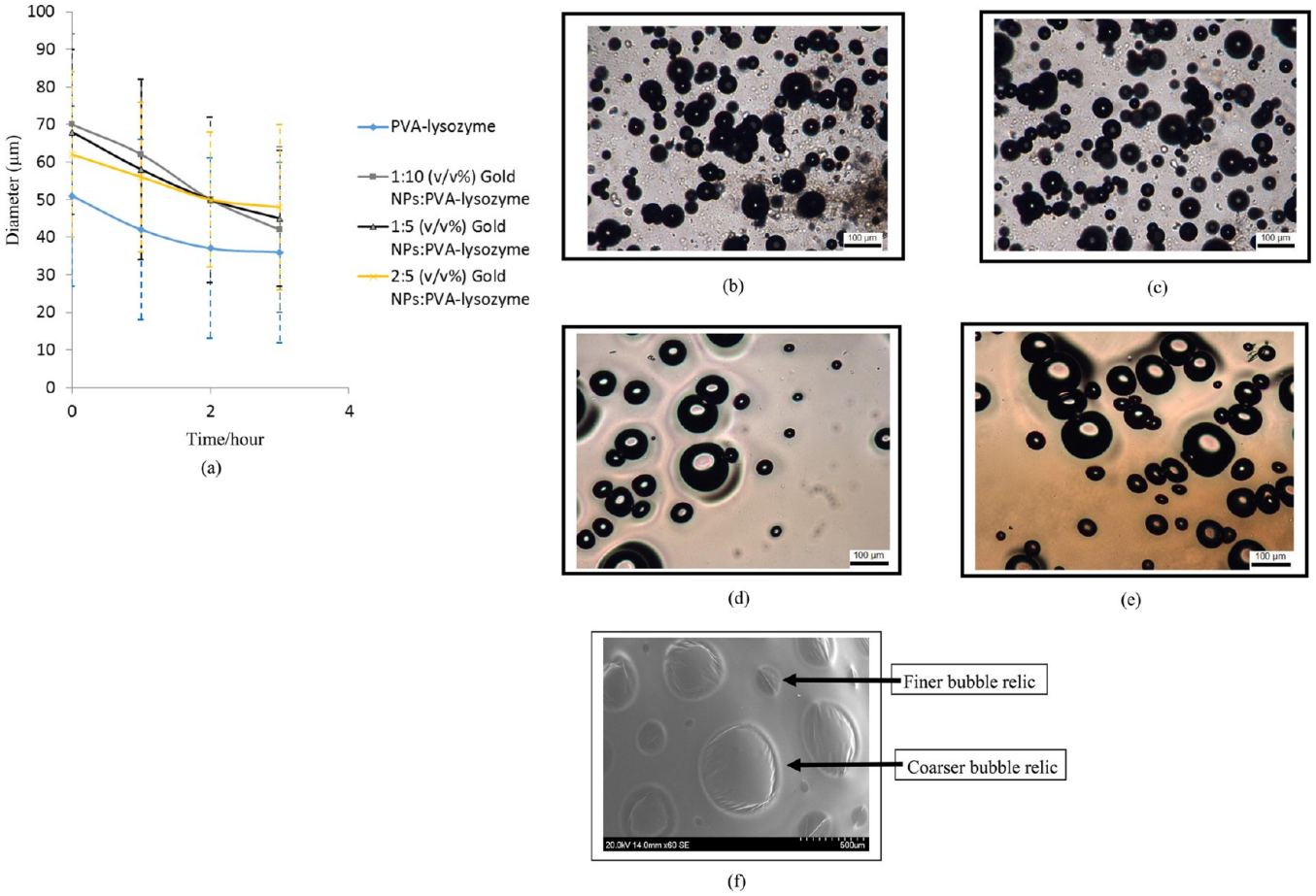

Figure 2. (a) Stability analysis of the microbubbles. (b)−(e) Optical micrographs of the PVA-lysozyme microbubbles at different times (hour): (b) 0, (c) 1, (d) 2, and (e) 3. (f) Field emission scanning electron microscope images of PVA-lysozyme microbubble relics.

viscosity of the polymer solutions was measured using a BrookField viscometer. All equipment was calibrated before use, and all measurements were performed at ambient temperature (~20 °C).

2.3. Bubble Preparation. The experimental setup used at ambient temperature in this study has been described in detail in our previous work.[19] Briefly, it consists of a rotary aluminum cylindrical vessel (~60 mm in diameter and ~35 mm in height) containing orifices (20) on its face. The size of one orifice is 0.5 mm. One end of the vessel was connected to a motor which can generate speeds of up to 36 000 rpm, while the other end was connected to a nitrogen gas stream, the pressure of which can be varied up to 3×10^5 Pa. The dynamics of the process has been studied in detail,[19] and the microbubbles evolve from the breakup of a jet which results from the rotating motion. To facilitate the collection of microbubbles, a stationary collector made of aluminum foil was placed around the spinning vessel. There was no deliberate attempt to control the bubble size and size distribution where the applications targeted (bacteria scavenging and biosensing) can tolerate coarser/polydisperse bubbles, unlike in ultrasound and drug delivery applications.

2.4. Structural Characterization. Microbubble samples deposited in the aluminum foil were collected using glass microscope slides. These were sealed in a Petri dish and maintained at ambient temperature. The microbubbles and their physical stability were observed using a Nikon Eclipse ME600 optical microscope over a period of 3 h. More than 100 microbubbles were studied using IMAGE J software (version 1.46r). The microbubbles were also characterized using the fluorescence microscope (EVOS FL) to verify the layer of gold nanoparticles on the shell of the microbubbles.

The relics of microbubbles formed were studied using field emission scanning electron microscopy (FE-SEM, model JSM 6301 F). Before imaging, samples were coated with carbon using an Edwards S1 50B sputter coater for 75 s. Ultraviolet−visible spectroscopy studies (UV−vis spectroscopy) were performed on the microbubble samples collected on glass slides using a PerkinElmer Lambda 35 spectrometer with a 4 nm spectral resolution at 25 °C in the 200−700 nm wavelength range.

2.5. Antibacterial Activity. The antibacterial activity of PVA-lysozyme and the gold nanoparticles containing PVA-lysozyme microbubbles was determined by staining and bacterial counting using *E. coli* as a model organism. Initially, the bacterial suspensions were prepared using a sterile laminar flow hood environment at ambient temperature. *E. coli* (6 μL) containing approximately 1×10^9 CFU/mL was diluted with 12 mL of Lauri-Bertani (LB) broth to create an *E. coli* suspension. At this point each of the different microbubble samples was divided into an equal volume to be added to each well in a 12-well plate, followed by 0.5 mL of the *E. coli* suspension. This allowed three repeats for each of the microbubble samples to be tested, in addition to three repeats of a control. The 12-well plate was then left to incubate in a shaking incubator for 3 h to allow thorough mixing of the microbubbles with the bacterial suspension. Thereafter, 1:10, 1:100, and 1:1000 dilutions of the incubated suspension containing *E. coli* and the samples were made. Tryptic soy agar Petri dishes were then used to inoculate the samples with varying concentrations. Each Petri dish was divided into quarters, 20 μL of different concentrations of a particular sample was dropped into the segment, and L-shaped plastic spreaders were used to distribute each drop into the shape of a quadrant. These Petri dishes were incubated at 38 °C for 24 h. Then, the Petri dishes were individually placed on the colony counter, and the bacteria were manually counted in order to calculate the antibacterial rate. The test is known as a 3 h test since this period of time represents the length of incubation time of *E. coli* and the samples, prior to the incubation of

DOI: 10.1021/acs.langmuir.5b02005
Langmuir 2015, 31, 9771−9780

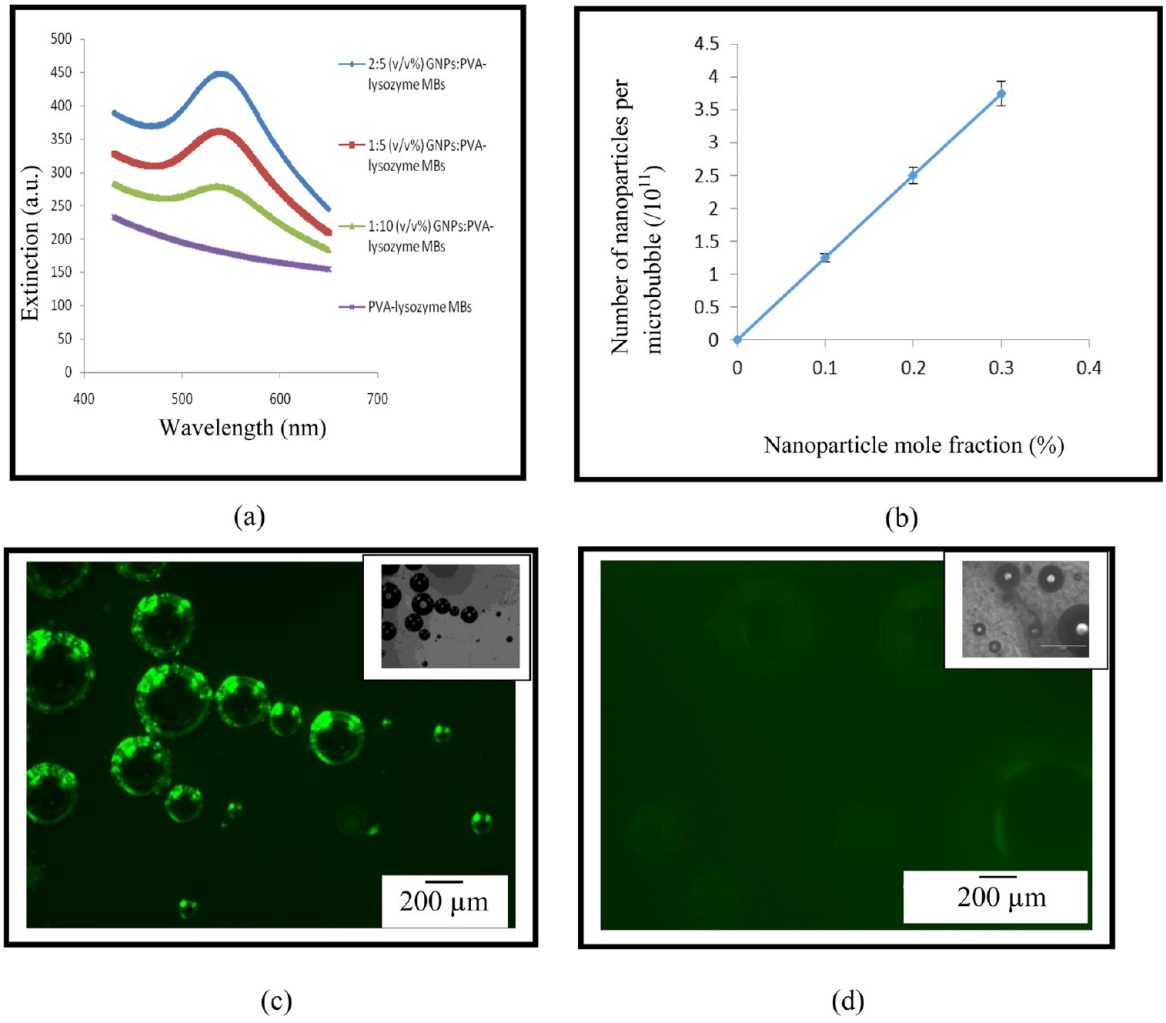

Figure 3. (a) Optical extinction phenomenon of microbubbles with and without gold nanoparticles (a.u. denotes arbitrary units). (b) Number of nanoparticles per microbubble as a function of gold nanoparticle concentration in solution. (c) Fluorescence microscopy image of the microbubbles containing gold nanoparticles. (d) Fluorescence microscopy image of the microbubbles without gold nanoparticles. (Insets in c and d show corresponding optical micrographs.)

the Petri dishes. The antibacterial rate was calculated where possible using the following equation

$$\text{antibacterial rate } (\%) = 100 \times \frac{A - B}{A} \quad (1)$$

where A is the average number of bacteria on the control (colony-forming units (CFU)/sample) sample and B is the average number of bacteria on the samples being tested (CFU/sample).

Fluorescence microscopy was also used to image the microbubbles after attachment to the bacterial cells. For this purpose the cultured microbubbles were stained with methylene blue (MB) in phosphate-buffered saline (PBS, pH ~7.2) and kept at 5 °C for 2 h. Then they were washed with PBS for 10 min and dried before imaging.

2.6. Biosensing. Biosensing characteristics of the PVA-lysozyme microbubbles were evaluated by the conjugation of alkaline phosphatase (AP) to the microbubbles. This was carried out by the reaction of 1 mg/mL microbubbles with 0.5 mg/mL malemide-functionalized AP (m-AP) in 50 mM PBS at pH 7.2 for 15 min at ambient temperature under gentle stirring. The reaction mixture was filtered out, and the remaining microbubbles were collected for biosensing characterization. The biosensing characteristics of m-AP-functionalized PVA-lysozyme microbubbles were evaluated by the detection of paraoxon which was used as a model compound in aqueous solution with and without p-NPP using a UV/vis spectrometer.

3. RESULTS AND DISCUSSION

The optical micrographs and the corresponding size distribution of the formed microbubbles under different rotation speeds and a constant working pressure of 0.2×10^5 Pa are shown in Figure 1. The working pressure has been chosen from the parametric plot constructed for the pressurized gyration of PVA-lysozyme solution as a function of rotational speed and working pressure.[19] The working pressure falls within the microbubble-forming region and is good enough to prepare bubbles at all rotation speeds. Microbubbles in the range of 10−250 μm were produced. Increasing rotational speed reduced the mean microbubble size. The polydispersity indices of the microbubble size distribution generated are 33, 40, and 57% for rotational speeds of 10 000, 24 000, and 36 000 rpm, respectively. Thus, increasing the rotational speed increased the polydispersity index and shows that the microbubble size and distribution could be controlled.

The stability analysis of the microbubbles is shown in Figure 2a. The mean bubble diameter decreased with holding time. The bubble diameter was nearly halved when the holding time increased from 0 to 3 h. The gold-nanoparticle-containing microbubbles were more stable than the PVA-lysozyme

DOI: 10.1021/acs.langmuir.5b02005
Langmuir 2015, 31, 9771−9780

microbubbles and this became more apparent as the gold nanoparticle concentration was increased. The gold nanoparticle concentration also influenced the stability of the microbubbles where more stable microbubbles were obtained with a higher concentration of the gold nanoparticles. Figure 2b−e shows the PVA-lysozyme microbubbles present at different times. Bubble relics were also studied with SEM (Figure 2f). The microbubbles are spherical and have a relatively smooth surface. The microbubbles constitute a thick shell, and there is no apparent change in the bubble surface due to gyration. It was initially thought that the shearing action of the gyration vessel might lead to deformed surfaces; however, these results show that there is no correlation between the bubble surface and the gyration process (Figure 2b,c). A closer examination of the microbubble surface after 2 and 3 h (Figure 2d,e) showed changes in shape and morphology. This is associated with the change in Laplace pressure over this period of time and the chemical modification of the shell of the microbubbles.[19]

The data in Figure 2 shows that the PVA-lysozyme microbubble diameter stabilized at ∼37 μm about 2 h after preparation. The stability of these microbubbles can be attributed to thermal denaturation where the PVA-lysozyme solution is heated to 80 °C prior to their preparation. The egg white lysozyme consists of 129 amino acids in the primary sequence and 4 intrachain disulfide bridges buried inside the hydrophobic core of the protein,[8] and the heating can break intrachain disulfide bonds to form free thiol groups. This could be attained by either chemical or thermal denaturation. In both cases the active thiol groups that are formed improve the formation as well as cross-linking properties that stabilize the microbubbles.[8] In addition, the chemical features of the PVA polymer chain in aqueous solutions form clusters of entangled chains stabilized by both hydrophobic interactions and intermolecular and intramolecular hydrogen bonds. The segregation of PVA at the shell of the microbubbles forms a backbone for the stabilization process (physical adsorption).[21]

The elasticity of the shell material is attributed to the stability of the microbubbles. Proteins can play a vital role in forming an elastic interface and a viscous elastic shell. This can be accomplished by the adsorption of proteins at the interface. The viscous nature of the shell arises from the rearrangements of intramolecules or intermolecules. When there is excess molecular interaction the interface becomes more elastic.[22] Moreover, the elasticity of the microbubble interface increases with the shell thickness. The greater the shell thickness, the higher the elasticity of microbubble shell. This improves the stability of the microbubbles by stopping the shrinkage due to disproportionation. In addition, a considerable amount of stability in the microbubbles can be achieved over a period of time from the intrabubble interaction. Moreover, microbubble disproportionation can be averted by interfacial viscosity which aids the stabilization process. Earlier work reports that there is no obvious effect of interfacial viscosity on the microbubble dissolution process when low interfacial viscosity prevails,[23] but the bubbles' shrinkage could be delayed. However, a greater stability of the microbubbles could be achieved by the presence of higher interfacial viscosity, which tremendously reduces bubble dissolution.[23]

The stability of microbubbles can be greatly improved by the adsorption of solid nanoparticles, i.e., gold in this work, on the bubble surfaces by a phenomenon called jamming.[24] This is identical to a well-known phenomenon called Pickering stabilization in liquid−liquid emulsions.[25] This behavior is also observed in foams.[26] The nanoparticles which possess significant adsorption energy can form a rigid shell at the interface of the microbubbles. These surface-active particles can stop microbubble shrinkage due to disproportionation. Therefore, by having a delicate balance between two tendencies, i.e., adsorption of the hydrophobic particles at the shell and the dispersion of particles in the liquid medium in which they are contained, improved stabilization can be obtained. In addition, there is some rearrangement of surface-active particles happening during disproportionation, and further adsorption of particles to the microbubble interface can take place, forming a more close-packed particle layer necessary for stability.[26]

The optical extinction spectra of the PVA-lysozyme and the gold nanoparticles containing PVA lysozyme microbubbles are shown in Figure 3a. They represent the optical scattering of the gas core and the absorption of the gold nanoparticles. The absorption by the gold nanoparticles is observed at a plasmon resonance frequency of ∼530 nm. The PVA-lysozyme microbubbles do not show any apparent peak, but in contrast, the gold-nanoparticle-containing PVA-lysozyme microbubbles showed a sharp peak. It is also seen that the sharpness and the extinction values changed with the concentration of the gold nanoparticles used. Figure 3b shows how the nanoparticles per microbubble can be varied with the mole fraction of the gold nanoparticles added to PVA-lysozyme. At 0.1 mol % the number of nanoparticles per microbubble is 1.25×10^{11}. As expected, the number of nanoparticles per microbubble increased with the concentration of the gold nanoparticles. Moreover, the higher surface area of the gold nanoparticles facilitated the binding of particles to the surface of microbubbles. The binding of gold nanoparticles to the surface of a microbubble was verified with fluorescence microscopy (Figure 3c). The brighter shell of the microbubbles (cf. Figure 3d) indicates the presence of gold nanoparticles.

The attachment of gold nanoparticles to the bubble surface is irreversible and stabilizes the surface. The formation of gold nanoparticles containing microbubbles depends on a delicate balance between the tendency of the hydrophobic particles to adsorb at microbubble surfaces and their tendency to aggregate rather than disperse in water. Moreover, microbubbles need to shrink appreciably to achieve stable disproportionation, and this suggests that during shrinkage there may be some rearrangement of the particles adsorbed on the microbubble surface and/or further adsorption of particles to the microbubbles, resulting in a more close-packed particle layer necessary for long-term stability.[26] In addition, the combination of rapid dissolution and slow particle transport and adsorption, coupled with bubbles of different sizes competing to capture the gold nanoparticles, gives rise to a rich variety of behaviors. For instance, the bubble size distribution varies with the number of nanoparticles available to bind in the shell layer before full stabilization is achieved. The magnitude of variation in the spread of the size distribution is also sensitive to the number of nanoparticles available.[27] Apart from being a very good stabilization agent, gold nanoparticles are well known for their biosensing applications.[28] It has been shown that gold nanoparticles binding to DNA have increased amplification and have been used to detect very low concentrations of thrombin.[28] Thus, biosensing is also investigated in this work.

The antibacterial properties of the microbubbles were evaluated using Gram-negative *E. coli* microorganisms. The interaction of the bacterial cells with the microbubble

DOI: 10.1021/acs.langmuir.5b02005
Langmuir 2015, 31, 9771−9780

suspension was captured in real time and is shown in the Supporting Information. Three samples from each PVA-lysozyme, gold-nanoparticle-containing PVA-lysozyme microbubbles, and control groups were investigated. Figure 4 shows

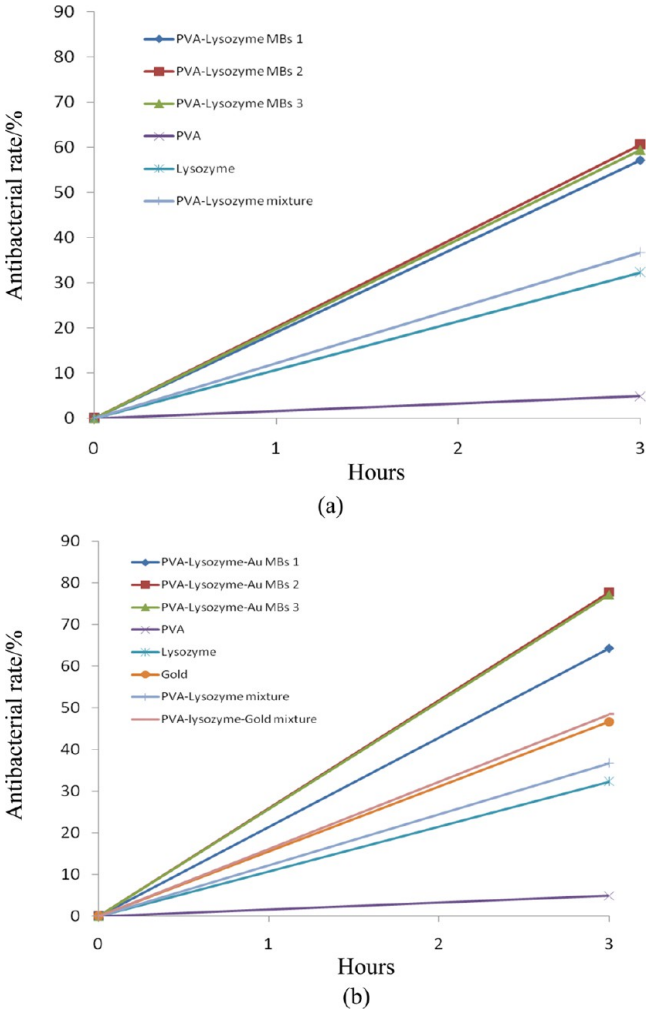

Figure 4. Antibacterial activity of microbubbles. (a) PVA-lysozyme and (b) gold-nanoparticle-containing PVA-lysozyme (2:5 v/v). The data for PVA is obtained from ref 43.

the plots of the antibacterial rate of the *E. coli* microorganisms after 3 h for PVA-lysozyme microbubbles and gold-nanoparticle-containing PVA-lysozyme microbubbles. As the contact time increased, the percentage (%) of bacterial colonies decreased. This is clearly exemplified in the Supporting Information video which shows the interaction of the bubbles and bacterial colonies. The average antibacterial rates after 3 h were ∼60% and ∼75% for PVA-lysozyme microbubbles and gold-nanoparticle-containing PVA-lysozyme microbubbles, respectively. The percentage reduction was higher for gold-nanoparticle-containing PVA-lysozyme microbubbles than for the PVA-lysozyme microbubbles. For gold-nanoparticle-containing PVA-lysozyme microbubbles, samples 2 and 3 have the same antibacterial rate whereas sample 1 has a different rate. This might be due to the variation of the accumulation time taken for bacterial cells to reach the microbubble surfaces. On the other hand PVA-lysozyme microbubbles have identical antibacterial rates for all three samples. Figure 5 shows the optical micrographs of the control group and the microbubbles containing a bacterial suspension. The typical morphology of *E. coli* shows rodlike shape and is consistent with earlier reports.[29] It is clearly seen that bacterial cell clusters were apparent in microbubbles containing a bacterial suspension (Figure 5b,c) compared to the control group (Figure 5a).

The antibacterial activity of PVA-lysozyme microbubbles is significantly higher than that of PVA and lysozyme solutions acting individually. For example, from Figure 4a, after 3 h, combining the PVA and lysozyme solutions gives an antibacterial rate of 37.2%, and the correponding experimental value is 36.7%. These values are significantly lower than that of the PVA-lysozyme microbubbles which have an average antibacterial rate of 59% after 3 h. The average antibacterial activity of the gold nanoparticle containing PVA-lysozyme microbubbles is 73% after 3 h (Figure 4b) and therefore clearly demonstrates the effect the gold nanoparticles had on the antibacterial activity. The bare gold nanoparticles give an antibacterial rate of 46.6% at 3 h. Therefore, the antibacterial activity of gold nanoparticles is higher than the PVA, lysozyme, and PVA-lysozyme mixture, and this is most probably due to the fact that gold nanoparticles have a higher surface area which promotes bacterial cell attachement and cell lysis. Individual addition of PVA, lysozyme, and gold nanoparticles gives a total antibacterial rate of 83.8% at 3 h. However, the experimental value of this mixture at the same time is 48.4%, which is significantly lower and indeed even lower than for the gold-nanoparticle-containing PVA-lysozyme microbubbles. But the value is considerably higher than for the PVA-lysozme mixture. Again, this shows the effect that gold nanoparticles had on the antibacterial activity. The reason for the lower antibacterial activity of the PVA-lysoyme-gold mixture compared to that of individual addition is that, in the mixture, the gold nanoparticles may be buried or coated with PVA-lysozyme solution that will hinder the exposure of the gold nanoparticle surface to bacterial cells, thus lowering the antibacterial activity. In addition, for effective antibacterial activity the gold nanoparticles have to be homogeneously distributed in the solution, and this is more effectively done in the microbubble suspension (i.e., on the surface, bubbles are decorated with gold nanoparticles) than in the PVA-lysozyme mixture.

It has been shown that denatured lysozyme is a potent antibactericidal agent against both Gram-negative and Gram-positive microorganisms.[30] Lysozyme is an antimicrobial enzyme characterized by a single polypeptide chain and by enzymatic activity against β-1,4 glycosidic bonds between *N*-acetylmuramic acid and *N*-acetylglucosamine.[31] Regardless of its enzyme activity, the lysozyme has been shown to possess antimicrobial activity.[8,30] In the denatured lysozyme, β-sheets are major structures holding the monomers in dimeric form. On the surface of the dimer, increased hydrophobicity and half-cystines contribute to the antibacterial action by increasing the permeability of the membrane.[30] Moreover, the reduction of disulfide bonds (S−S) could expose many hydrophobic groups and tryptophan (Trp) residues, enabling the microbubbles to interact with the bacterial membrane.[32] In addition, by triggering autolysin activity, lysozyme may kill the bacteria. Autolysins are a subset of peptidoglycan-synthesizing enzymes, the activation of which causes bacteria to form the faulty peptidoglycan and lyse.[33] The bacterial cell wall tends to attract positively charged lysozyme microbubbles because of the total charge of the cell wall being negative, and thus the cell wall under high stress can cause immediate cell lysis.

DOI: 10.1021/acs.langmuir.5b02005
Langmuir 2015, 31, 9771−9780

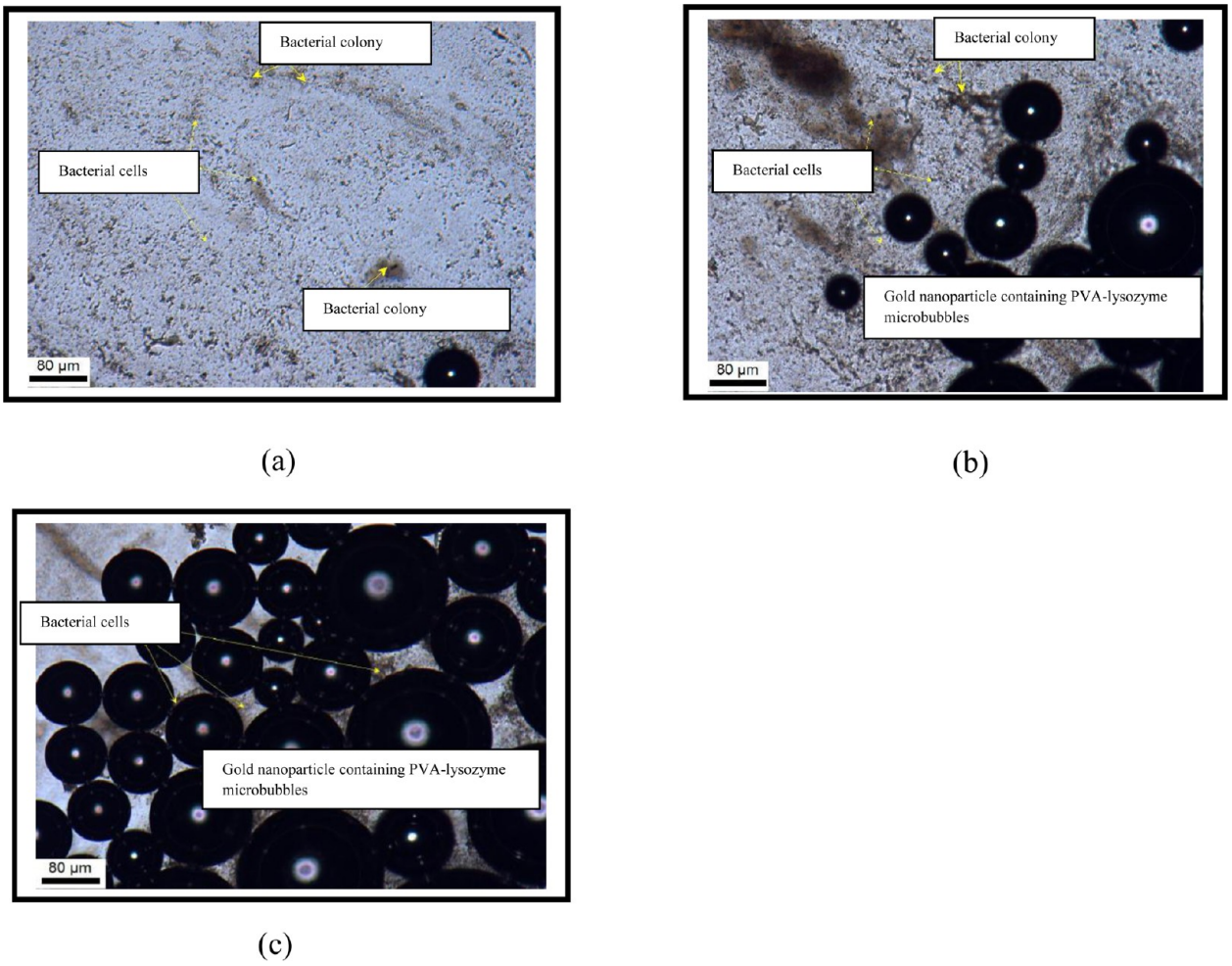

Figure 5. Optical micrographs of (a) the control group (*E. coli* suspension), (b) the interaction of microbubbles with an *E. coli* suspension, and (c) stable microbubbles leading to cell lysis on the surface of the microbubbles.

It is also worth mentioning here that comparing the antibacterial activity of lysozyme solution with the lysozyme microbubbles is not meaningful since most of the protein in the microbubble is buried within the shell of the microbubble.[8] It is interesting to see that gold-nanoparticle-containing PVA-lysozyme microbubbles have higher antibacterial activity than the PVA-lysozyme microbubbles. The gold nanoparticle interacts with the cell membrane of *E. coli* and forms a distinct aggregation pattern and lysis of bacterial cells.[34] Also, the blebbing caused by cationic gold nanoparticles induces bacterial membrane damage.[35] The antibacterial activity of the gold nanoparticles depends on the specific surface area. The gold nanoparticles possess a higher surface area and can attach more cell membranes to its surface and disturb its power function such as permeability and respiration.[36] Moreover, the electrostatic interaction between the gold nanoparticle and the cell surface induces stress in the membranes, which leads to cell damage.[37]

The biosensing characteristics of the PVA-lysozyme microbubbles were evaluated by the conjugation of m-AP to the bubble surface and thereafter detection of the paraoxon analyte at very low concentrations. Paraoxon is an organophosphorous (OP) pesticide widely used as an insecticide which adversely affects the human brain and tissues. These compounds are structurally very similar to nerve gases and are well known for their inhibition of acetylcholinesterase, which is responsible for transmitting nerve impulses across synaptic junctions.[38] The OP compounds are poisonous when inhaled, ingested, or absorbed through the skin. Therefore, the development of sensors capable of detecting harmful concentrations of these compounds would be beneficial to humans and livestock populations.[39] The AP catalyzes the hydrolysis of phenyl phosphates to phenols.

The calibration curve for the biosensing process is shown in Figure 6a. Initially absorbance is obtained at various concentrations of paraoxon with and without p-NPP. The degree of inhibition of paraoxon with respect to the enzymatic activity of AP was measured as the relative decrease in absorbance observed after mixing microbubbles and paraoxon. This has been shown schematically in Figure 6b. The difference in absorbance is plotted against the analyte paraoxon concentration. The absorbance varies linearly with the paraoxon concentration. A 20% competitive inhibition of enzymatic activity was observed for m-AP functionalized with PVA-lysozyme microbubbles with 0.5 ppm paraoxon. A wide variety of techniques such as gas chromatography, high-performance liquid chromatography, and electrochemical methods have been devised to detect the presence of OP compounds, and these techniques are time-consuming, expensive, and complex. To overcome these problems, enzymatic bioassays have been designed for enhanced detection, high efficiency, and sensitivity to OP compounds.[40]

DOI: 10.1021/acs.langmuir.5b02005
Langmuir 2015, 31, 9771−9780

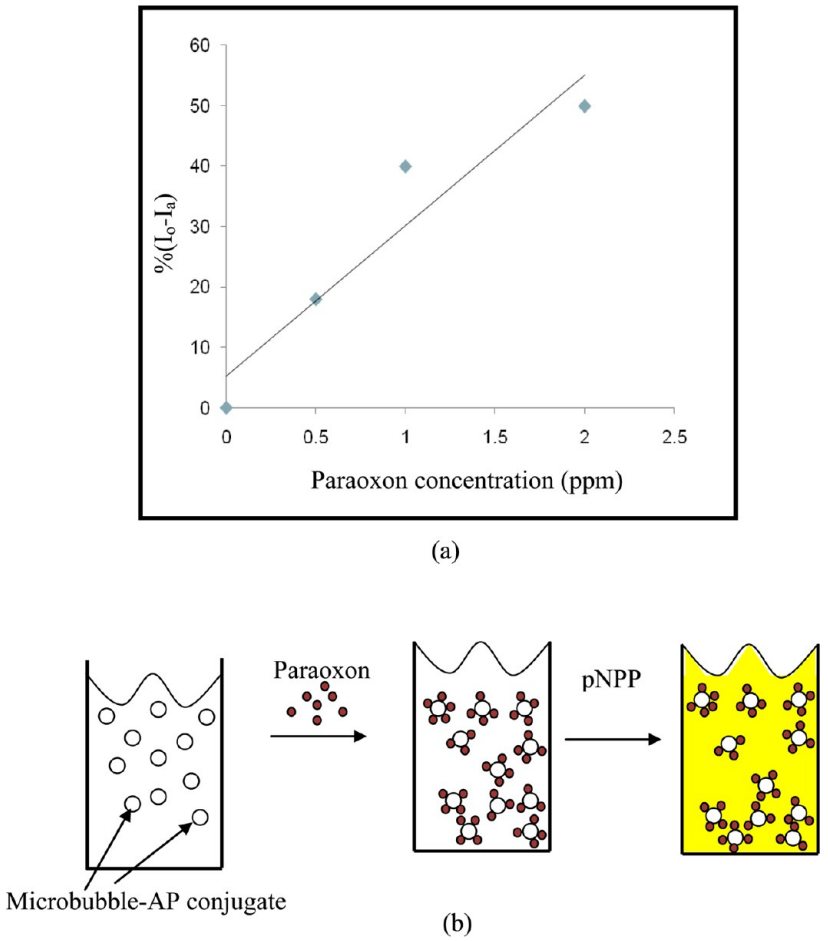

Figure 6. (a) Calibration curve for paraoxon. I_o represents absorbance without inhibitor (p-NPP), and I_a represents absorbance with inhibitor. (b) Schematic showing the behavior of paraoxon in solution of AP-conjugated microbubbles.

The enzymatic bioassay based on microbubbles developed and presented here is equivalent to the higher detection limit of paraxon obtained by colorimetric detection.[41] More importantly, it satisfies the requirement of the current pesticide residue standard of the European Union for the detection of paraoxon.[41] In addition, these microbubble-based bioassays show better detection capability than the semiconductor CdSe-based biosensors[42] and are cheaper and easier to handle. Therefore, designing and engineering such a functional system could be used over a broad application area including diagnostic tools and environmental bioassays. In addition, optical, magnetic, and potentially plasmonic functionalities may be embedded within the microbubbles to explore a wide range of healthcare applications.

4. CONCLUSIONS

Bubbles up to 250 μm in diameter were produced by pressurized gyration using a series of protein solutions (PVA-lysozyme), and the bubble diameter was reduced by increasing the rotational speed. A unimodal size distribution was obtained for all of the rotational speeds at a constant working pressure which was selected appropriately to form microbubbles from the PVA-lysozyme system. The mean microbubble size was reduced from ~100 to ~50 μm when increasing the rotational speed from 10 000 to 36 000 rpm. The optical extinction values of the gold-nanoparticle-containing microbubbles were higher than for the bare protein microbubbles. These values increased with the increase in concentration of the gold nanoparticles and reached 450, a 4-fold increase, at a gold nanoparticle concentration of 40%. The antibacterial activity of the protein microbubbles was tested with the Gram-negative *E. coli* microorganism, and increased activity was found for gold-nanoparticle-containing microbubbles compared to that of the bare protein microbubbles. The average antibacterial activity for gold-nanoparticle-containing microbubbles was found to be 73% whereas bare protein microbubbles showed 59% activity. The mechanisms of antibacterial activity include the interaction of positively charged lysozyme microbubbles with the negatively charged cell wall, thus putting the cell wall under high stress which can cause immediate cell lysis. The biosensing capabilities of the microbubbles prepared were also investigated using paraoxon. The detection of paraoxon levels of as low as 0.5 ppm was possible with alkaline phosphatase-conjugated microbubbles, and this demonstrates a better detection capability than with other bioassays.

■ ASSOCIATED CONTENT

Supporting Information

The Supporting Information is available free of charge on the ACS Publications website at DOI: 10.1021/acs.langmuir.5b02005.

Gold nanoparticles containing PVA-lysozyme microbubbles (AVI)

DOI: 10.1021/acs.langmuir.5b02005
Langmuir 2015, 31, 9771−9780

AUTHOR INFORMATION

Corresponding Author

*E-mail: m.edirisinghe@ucl.ac.uk. Tel: +442076793920.

Notes

The authors declare no competing financial interest.

ACKNOWLEDGMENTS

We are grateful for an Engineering and Physical Sciences Research Council (EPSRC)-UCL Knowledge Exchange Programme Award which initiated this work and helped to attract Z.X, a privately funded Ph.D. researcher. S.M. is supported by EPSRC grant EP/L 023059/1. We also thank Dr. Raimi-Abraham of the UCL School of Pharmacy for helping to prepare the lysozyme protein solutions. We are very grateful to Dr. Jennifer Rohn from the Centre for Clinical Science and Technology, Division of Medicine, University College London for allowing Z.X. to use her experimental facilities for antibacterial studies. Data supporting this study are provided in the paper and as Supporting Information accompanying this paper.

REFERENCES

(1) Guo, G.; Lu, L.; Yin, L.; Tu, Y.; Guo, X.; Wu, J.; Xu, D.; Zhang, D. Mechanical and dynamic characteristics of encapsulated microbubbles coupled by magnetic nanoparticles as multifunctional imaging and drug delivery agents. *Phys. Med. Biol.* **2014**, *59*, 6729−6747.

(2) Angile, F. E.; Vargo, K. B.; Sehgal, C. M.; Hammer, D. A.; Lee, D. Recombinant protein-stabilised monodisperse microbubbles with tunable size using a valve-based microfluidic device. *Langmuir* **2014**, *30*, 12610−12618.

(3) Rix, A.; Palmowski, M.; Gremse, F.; Palmowski, K.; Lederle, W.; Kiessling, F.; Bzyl, J. Influence of repetitive contrast agent injections on functional and molecular ultrasound measurements. *Ultrasound Med. Biol.* **2014**, *40*, 2468−2475.

(4) Cool, S. K.; Geers, B.; Roels, S.; Stremersch, S.; Vanderperren, K.; Saunders, J. H.; De Smedt, S. C.; Demeester, J.; Sanders, N. N. Coupling of drug containing liposomes to microbubbles improves ultrasound triggered drug delivery in mice. *J. Controlled Release* **2013**, *172*, 885−893.

(5) Whitesides, G. The Origins and the Future of Microfluidics. *Nature* **2006**, *442*, 368−373.

(6) Hernot, S.; Klibanov, A. L. Microbubbles in ultrasound-triggered drug and gene delivery. *Adv. Drug Delivery Rev.* **2008**, *60*, 1153−1166.

(7) Zhu, C.; He, N.; Cheng, T.; Tan, H.; Guo, Y.; Chen, D.; Cheng, M.; Yang, Z.; Zhang, X. Ultrasound-targeted microbubble destruction enhances human β-defensin 3 activity against antibiotic-resistant Staphylococcus biofilms. *Inflammation* **2013**, *36*, 983−996.

(8) Cavalieri, F.; Ashokkumar, M.; Grieser, F.; Caruso, F. Ultrasonic synthesis of stable, functional lysozyme microbubbles. *Langmuir* **2008**, *24*, 10078−10083.

(9) He, N.; Hu, J.; Liu, H.; Zhu, T.; Huang, B.; Wang, X.; Wu, Y.; Wang, W.; Qu, D. Enhancement of vancomycin activity against biofilms by using ultrasound-targeted microbubble destruction. *Antimicrob. Agents Chemother.* **2011**, *55*, 5331−5337.

(10) Halford, A.; Ohl, C.-D.; Azarpazhooh, A.; Basrani, B.; Friedman, S.; Kishen, A. Synergetic effect of microbubble emulsion and sonic or ultrasonic agitation on endodontic biofilm in Vitro. *J. Endodont.* **2012**, *38*, 1530−1534.

(11) Shimanovich, U.; Cavaco-Paulo, A.; Nitzan, Y.; Gedanken, A. Sonochemical coating of cotton and polyester fabrics with antibacterial BSA and Casein microspheres. *Chem. - Eur. J.* **2012**, *18*, 365−369.

(12) Sun, C.; Zhao, X.-W.; Zhao, Y.-J.; Zhu, R.; Gu, Z.-Z. Fabrication of colloidal crystal beads by a drop-breaking technique and their application as bioassay. *Small* **2008**, *4*, 592−596.

(13) Vong, F.; Son, Y.; Bhuiyan, S.; Zhou, M.; Cavalieri, F.; Ashokkumar, M. A comparison of the physical properties of ultrasonically synthesized lysozyme- and BSA-shelled microbubbles. *Ultrason. Sonochem.* **2014**, *21*, 23−28.

(14) Mahalingam, S.; Meinders, M. B. J.; Edirisinghe, M. Formation, stability, and mechanical properties of bovine serum albumin stabilised air bubbles produced using coaxial electrohydrodynamic atomization. *Langmuir* **2014**, *30*, 6694−6703.

(15) Mohamedi, G.; Azmin, M.; Pastoriza-Santos, I.; Huang, V.; Perez-Juste, J.; Liz-Marzan, L. M.; Edirisinghe, M.; Stride, E. Effects of gold nanoparticles on the stability of microbubbles. *Langmuir* **2012**, *28*, 13808−13815.

(16) Dressaire, E.; Bee, R.; Bell, D. C.; Lips, A.; Stone, H. A. Interfacial polygonal nanopatterning of stable microbubbles. *Science* **2008**, *320*, 1198−1200.

(17) Park, J. I.; Tumarkin, E.; Kumacheva, E. Small, stable and monodispersed bubbles encapsulated with biopolymers. *Macromol. Rapid Commun.* **2010**, *31*, 222−227.

(18) Forsberg, F.; Lathia, J. D.; Merton, D. A.; Liu, J.-B.; Le, N.; Goldberg, B. B.; Wheatley, M. A. Effect of shell type on the in vivo backscatter from polymer-encapsulated microbubbles. *Ultrasound Med. Biol.* **2004**, *30*, 1281−1287.

(19) Mahalingam, S.; Raimi-Abraham, B.; Duncan, Q. C. M.; Edirisinghe, M. *Langmuir* **2015**, *31*, 659−666.

(20) Mahalingam, S.; Edirisinghe, M. J. Forming of Polymer Nanofibres by a Pressurised Gyration Process. *Macromol. Rapid Commun.* **2013**, *34*, 1134−1139.

(21) Cavalieri, F.; Hamassi, A. E.; Chiessi, E.; Paradossi, G. Stable polymeric microballoons as multifunctional device for biomedical uses: synthesis and characterisation. *Langmuir* **2005**, *21*, 8758−8764.

(22) Meinders, M. B. J.; Kloek, W.; van Vliet, T. Effect of surface elasticity on Ostwald ripening in emulsions. *Langmuir* **2001**, *17*, 3923−3929.

(23) Kloek, W.; van Vliet, T.; Meinders, M. B. J. Effect of bulk and interfacial rheological properties on bubble dissolution. *J. Colloid Interface Sci.* **2001**, *237*, 158−166.

(24) Subramaniam, A.; Mejean, C.; Abkarian, M.; Stone, H. A. Microstructure, morphology and life time of armored bubbles exposed to surfactants. *Langmuir* **2006**, *22*, 5986−5990.

(25) Pickering, S. Emulsions. *J. Chem. Soc., Trans.* **1907**, *91*, 2001−2021.

(26) Du, Z. P.; Bilbao-Montoya, M. P.; Binks, B. P.; Dickinson, E.; Ettelaie, R.; Murray, B. S. Outstanding stability of particle-stabilised bubbles. *Langmuir* **2003**, *19*, 3106−3108.

(27) Ettelaie, R.; Murray, B. S. Evolution of bubble distribution in particle stabilised bubble dispersions: Competition between particle adsorption and dissolution kinetics. *Colloids Surf., A* **2015**, *475*, 27−36.

(28) Qiu, H.; Sun, Y.; Huang, X.; Qu, Y. A sensitive nanoporous gold-based electrochemical aptasensor for thrombin detection. *Colloids Surf., B* **2010**, *79*, 304−308.

(29) Jin, G.; Qin, H.; Cao, H.; Qian, S.; Zhao, Y.; Peng, X.; Zhang, X.; Liu, X.; Chu, P. K. Synergetic effects of dual Zn/Ag ion implantation in osteogenic activity and antibacterial ability of titanium. *Biomaterials* **2014**, *35*, 7699−7713.

(30) Ibrahim, H. R.; Higashiguchi, S.; Juneja, L. R.; Kim, M.; Yamamoto, T. A structural phase of heat-denatured lysozyme with novel antimicrobial action. *J. Agric. Food Chem.* **1996**, *44*, 1416−1423.

(31) Cavalieri, F.; Micheli, L.; Kaliappan, S.; Teo, B. M.; Zhou, M.; Palleschi, G.; Ashokkumar, M. Antimicrobial and biosensing ultrasound-responsive lysozyme-shelled microbubbles. *ACS Appl. Mater. Interfaces* **2013**, *5*, 464−471.

(32) Touch, V.; Hayakawa, S.; Saitoh, K. Relationship between conformational changes and antimicrobial activity of lysozyme upon reduction of its disulfide bonds. *Food Chem.* **2004**, *84*, 421−428.

(33) Ibrahim, H. R.; Higashiguchi, S.; Koketsu, M.; Juneja, L. R.; Kim, M.; Yamamoto, T.; Sugimoto, Y.; Aoki, T. Partially unfolded lysozyme at neutral pH agglutinates and kills gram-negative and gram-positive bacteria through membrane damage mechanism. *J. Agric. Food Chem.* **1996**, *44*, 3799−3806.

(34) Li, X.; Robinson, S. M.; Gupta, A.; Saha, K.; Jiang, Z.; Moyano, D. F.; Sahar, A.; Riley, M. A.; Rotello, V. M. Functional gold

DOI: 10.1021/acs.langmuir.5b02005
Langmuir 2015, 31, 9771−9780

nanoparticles as potent antimicrobial agents against multi-drug-resistance bacteria. *ACS Nano* **2014**, *8*, 10682−10686.
(35) Zhao, Y. Y.; Tian, Y.; Cui, Y.; Liu, W. W.; Ma, W. S.; Jiang, X. Y. Small molecule-capped gold nanoparticles as potent antibacterial agents that target gram-negative bacteria. *J. Am. Chem. Soc.* **2010**, *132*, 12349−12356.
(36) Bindhu, M. R.; Umadevi, M. Silver and gold nanoparticles for sensor and antibacterial applications. *Spectrochim. Acta, Part A* **2014**, *128*, 37−45.
(37) Bindhu, M. R.; Umadevi, M. Antibacterial activities of green synthesized gold nanoparticles. *Mater. Lett.* **2014**, *120*, 122−125.
(38) Raushel, F. M. Bacterial detoxification of organophosphate nerve agents. *Curr. Opin. Microbiol.* **2002**, *5*, 288−295.
(39) Chen, C.-H.; Yang, K.-L. A liquid crystal biosensor for detecting organophosphates through the localized pH changes induced by their hydrolytic products. *Sens. Actuators, B* **2013**, *181*, 368−374.
(40) Orbulescu, J.; Constantine, C. A.; Rastogi, V. K.; Shah, S. S.; DeFrank, J. J.; Leblanc, R. M. Detection of organophosphorus compounds by covalently immobilised organophosphorus hydrolase. *Anal. Chem.* **2006**, *78*, 7016−7021.
(41) Fu, G.; Chen, W.; Yue, X.; Jiang, X. Highly sensitive colorimetric detection of organophosphate pesticides using copper catalyzed click chemistry. *Talanta* **2013**, *103*, 110−115.
(42) Ji, X.; Zheng, J.; Xu, J.; Rastogi, V. K.; Cheng, T.-C.; DeFrank, J. J.; Leblanc, R. M. (CdSe)ZnS quantum dots and organophosphorus hydrolase bioconjugate as biosensors for detection of paraoxon. *J. Phys. Chem. B* **2005**, *109*, 3793−3799.
(43) Galya, T.; Sedlarik, V.; Kuritka, I.; Novotny, R.; Sedlarikova, J.; Saha, P. Antibacterial polyvinyl (alcohol) film containing silver nanoparticles: Preparation and Characterisation. *J. Appl. Polym. Sci.* **2008**, *110*, 3178−3185.

DOI: 10.1021/acs.langmuir.5b02005
Langmuir 2015, 31, 9771−9780